A highly sensitive electrochemical sensor for nitrite detection based on Fe$_2$O$_3$ nanoparticles decorated reduced graphene oxide nanosheets

Sivaprakasam Radhakrishnan [a,b], Karthikeyan Krishnamoorthy [a], Chinnathambi Sekar [b], Jeyaraj Wilson [b], Sang Jae Kim [a,*]

[a] Nanomaterials and System Lab, Department of Mechanical System Engineering, Jeju National University, Jeju 690-756, Republic of Korea
[b] Department of Bioelectronics and Biosensors, Alagappa University, Karaikudi 630 003, Tamil Nadu, India

ARTICLE INFO

ABSTRACT

Nitrite is one of the most frequent measurements in environmental analysis due to their detrimental effect on environment. The development of simple and sensitive analytical method for the detection of nitrite is highly important. In this study, we report the fabrication and testing of nitrite sensor based on the use of Fe$_2$O$_3$/rGO composite. The Fe$_2$O$_3$/rGO composites were prepared by a facile one-step hydro-thermal approach. Field emission scanning electron microscope studies and powder X-ray diffraction analysis revealed that the Fe$_2$O$_3$ nanoparticles were successfully grafted on the rGO nanosheets. Further, the prepared Fe$_2$O$_3$/rGO composites have been examined for the electrochemical detection of nitrite using cyclic voltammetry and differential pulse voltammetry techniques. The electrochemical studies demonstrated that Fe$_2$O$_3$/rGO composite detects nitrite linearly over a concentration range of 5.0×10^{-8} to 7.8×10^{-4} M with a detection limit of 1.5×10^{-8} M. The obtained detection limit for Fe$_2$O$_3$/rGO composite is very much comparable to the recent literature values. Furthermore, the Fe$_2$O$_3$/rGO composite modified electrode showed an excellent anti-interference ability against electroactive species and metal ions.

1. Introduction

Highly sensitive detection of nitrite (NO$_2^-$) has attracted increasing attention in the past decades due to their detrimental effect on both environment and human health. The rapid increasing pollution of ground water resources for human consumption by nitrites due to the anthropogenic activities from agriculture (by using nitrogen based fertilizer) and waste water from industry is receiving worldwide attention [1–4]. The World Health Organization has fixed the maximum limit of 3 mg L^{-1} for nitrite in drinking water [5]. Nitrite contamination in drinking water can cause different diseases such as methemoglobinemia or "Blue Baby Syndrome" and stomach cancer by the formation of N-nitrosamines when nitrite ions interact with amines [6–8]. Therefore, it is of great importance to accurately monitor nitrite for public health, environmental and food industries. Several analytical techniques have been developed for nitrite determination including spectrophotometry [9], chemiluminescence [10], capillary electrophoresis [11] and chromatography [12]. However, these analytical methods usually have expensive equipments, tedious detection procedure and often

time consuming. Compared to these methods, the electrochemical method can provide compact, relatively inexpensive, reliable, sensitive and real-time analysis [13,14]. Moreover, the development of a rapid electrochemical method for nitrite detection without the sample pretreatment prior to analysis and also no interference from other sources (such as nitrate, sulfate, bromate ions and oxygen) is highly important. Recently, different kinds of electrochemical nitrite sensors have been fabricated based on the chemical modification of electrode [15–19].

Carbon nanostructures (fullerenes, carbon nanotubes and graphene) have been extensively used in electrochemistry due to the small residual current, wide potential window, excellent chemical stability in various electrolytes and easy renewable surface. It is well known that graphene (an ideal two-dimensional layered material) has been extensively used for growing and anchoring of metal oxide nanoparticles due to their unique physical and chemical properties. In this decade, metal oxide/graphene composite materials (SnO$_2$/graphene, Cu$_2$O/graphene, Co$_3$O$_4$/graphene, *etc.*,) have attracted a great deal of attention due to their improved electrochemical properties [20–22]. Recently, Zhang et al. [23], prepared the sensor of Cu dendrites and reduced graphene oxides, which displayed electrocatalytic activity to the detection of nitrite. Zhang et al. [24], reported the electrochemical synthesis of reduced graphene oxide/palladium nanocomposite on GC electrode, and

* Corresponding author. Tel.: +82 64 754 3715; fax: +82 64 756 3886.
E-mail address: kimsangj@jejunu.ac.kr (S.J. Kim).

proposed film showed good electrocatalytic activity toward oxidation of nitrite. Cui et al. [25], fabricated a composite film containing graphene nanosheets and carbon nanospheres, and then they studied its electrochemical properties, and electrocatalytic activity toward the nitrite oxidation in the presence of chitosan coated Prussian blue as redox mediator.

Hematite (Fe_2O_3), as an important n-type metal oxide with a narrow band gap ($E_g = 2.2$ eV), has received considerable attention in recent years due to its low cost, non-toxicity, easy of production and easy of storage. It has been deeply investigated because of its wide applications in catalysts, pigments, magnetic materials, gas sensors, biosensors and lithium ion batteries [26–30]. Several approaches have been used to synthesis metal oxide/graphene sheets hybrids; pyrolysis, thermal annealing, chemical reduction, microwave irradiation and sonochemical [31–35]. Further, these processes involve two steps, which involve the reduction of graphene sheets by thermal annealing or adding toxic hydrazine. Hence, these methods are obviously involving complicated experimental protocol with high energy consuming and sophisticated instrumentation techniques. Therefore, facile material preparation and electrode modification protocol with improved catalytic performance of nitrite is urgently required.

In this paper, we report the fabrication, characterization and analytical performance of a nitrite sensor based on the Fe_2O_3/reduced graphene oxide (rGO) composite modified glassy carbon (GC) electrode by a very simple technique. The Fe_2O_3/rGO composites were synthesized in ethanol by a one-step hydrothermal approach and used for the sensitive detection of nitrite for the first time. The performance of the newly fabricated nitrite sensor was studied using cyclic voltammetry (CV), electrochemical impedance spectroscopy (EIS) and differential pulse voltammetry (DPV) and the results are discussed. The fabricated sensor showed high sensitivity, stability and satisfactory reproducibility.

2. Experimental

2.1. Materials

Ferrous chloride and ammonia are purchased from Daejung Chemicals Ltd, South Korea. Sodium nitrite is obtained from Sisco Research Laboratories, India. The phosphate buffer solutions with different pH values were prepared using Na_2HPO_4 and NaH_2PO_4. All the reagents were of analytical grade and used without further purification.

2.2. Instrumentation

The surface morphologies of the prepared materials were characterized using a field emission-scanning electron microscope (FE-SEM) JEOL JSM-6700F. The phase purity and crystalline nature of the prepared materials were studied using the powder X-ray diffraction technique (XRD, Rigaku, Cu Kα radiation operating at 40 KeV/40 mA). FT-IR spectra were recorded using nicolet-6700 spectrometer from Thermo Scientific. Electrochemical measurements were performed in a conventional two compartment three electrode cell with a mirror polished 3 mm glassy carbon (GC) as the working electrode, Pt wire as the counter electrode and an Ag/AgCl (3 M KCl) as the reference electrode. The electrochemical measurements were carried out with an AUTOLAB (Model PGSTAT302N, Netherlands). Cyclic voltammograms were recorded between a potential window of −0.2 V and 0.6 V at a scan rate of 50 mV s^{-1} in 0.1 M KCl solution containing 1.0 mM [Fe(CN)$_6$]$^{3-/4-}$ redox couple. The electrochemical impedance spectroscopy (EIS) measurements were carried out by applying an ac potential of amplitude 10 mV over the dc potential of 200 mV in the frequency range of 100 kHz–1 Hz. The impedance data are presented in the form of Nyquist plots. The value of the charge transfer resistance (R_{ct}) was determined using Zsimpwin software simulations. The DPV measurements were performed in the potential region from 0.4 to 1.0 V in PBS (pH 7.0) at a scan rate of 10 mV s^{-1} with amplitude of 0.025 V and a step potential of 0.05 V.

2.3. Preparation of Fe_2O_3/rGO composite

Graphene oxide (GO) was synthesized from graphite powders by a modified Hummers method as described in our earlier report [36]. The Fe_2O_3/rGO nanocomposites were prepared by a hydrothermal method similar to the one reported earlier [37]. Briefly, 50 mg graphene oxide was dispersed in 70 mL ethanol and ultrasonicated for 30 min. Then, 0.1 g FeCl$_2$ and 25% ammonia (100 μL) were added into the solution. Afterwards, the mixture was sealed into a Teflon-lined stainless steel autoclave and maintained at 170 °C for 4 h and then cooled to room temperature gradually. Subsequently, the precipitation was filtered, washed with distilled water and ethanol several times, and dried at 80 °C for 6 h in a vacuum oven. For comparison, pure Fe_2O_3 and reduced graphene oxide (rGO) were prepared by the same method.

2.4. Fe_2O_3/rGO composite modified electrode

The Fe_2O_3/rGO composite modified GC electrode was prepared as follows. First, the surface of the glassy carbon (GC) electrode for each experiment was mechanically polished with alumina suspensions (0.5 and 1.0 μM respectively). After that, the electrode was successively washed in ethanol and water for 2 min by ultrasonic method. A 10 μL aliquot of Fe_2O_3/rGO composite (dispersion in water, 0.5 mg mL^{-1}) was dropped onto the surface of GC electrode and dried under room temperature (Scheme 1). In addition, rGO and Fe_2O_3 modified GC electrodes were prepared by the above mentioned process for comparison.

3. Results and discussion

3.1. Characterization of the as-prepared Fe_2O_3/rGO composite

The microstructure and morphology of the GO, rGO, Fe_2O_3/rGO composite and Fe_2O_3 were characterized by FE-SEM. Fig. 1 shows the FE-SEM micrographs of the GO (A) and rGO (B), in which the GO and rGO appears corrugated into a wrinkle shape. Fig. 1C shows the Fe_2O_3/rGO composite, it can be seen that the Fe_2O_3 nanoparticles were well decorated on the reduced graphene oxide sheets. These results clearly indicate the presence of strong interaction between rGO and Fe_2O_3 nanoparticles. The highly dispersed metal oxide nanoparticles on high surface area of reduced graphene oxide nanosheet may create a better communication between the electrode and analyte. Fig. 1D shows the Fe_2O_3 nanoparticles made under identical condition without the GO. Comparison of Fig. 1C and D reveals that the average size of the Fe_2O_3 nanoparticles formed is 100 ± 10 nm.

The crystalline nature of the rGO/Fe_2O_3 composite was investigated by powder XRD method. Fig. 2a–d shows the XRD pattern of GO, rGO, Fe_2O_3/rGO composite and Fe_2O_3, respectively. As seen in Fig. 2a, GO has two peaks that appear at $2\theta = 10.35°$ and $42.1°$, corresponding to the (0 0 1) and (1 1 1) diffraction planes, which is identical with reported values [38]. In Fig. 2b, an intense peak at $2\theta = 24.2°$ can be observed, while a peak of $2\theta = 10.35°$ has disappeared, which highlights that oxygen-containing functional groups have been removed during the reduction of GO into rGO. The XRD pattern of the Fe_2O_3/rGO composite (Fig. 2c) shows the presence of well-defined peaks that are centered at ca. 23.9°, 33°, 35.4°, 40.7°, 49.3°, 53.9°, 57.4°, 62.3° and 63.9°, where all the diffraction peaks
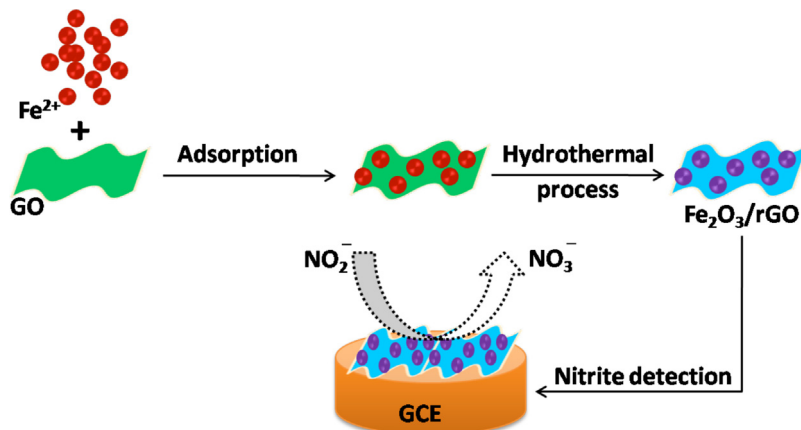
Scheme 1. Nitrite detection scheme using Fe_2O_3/rGO modified glassy carbon electrode.
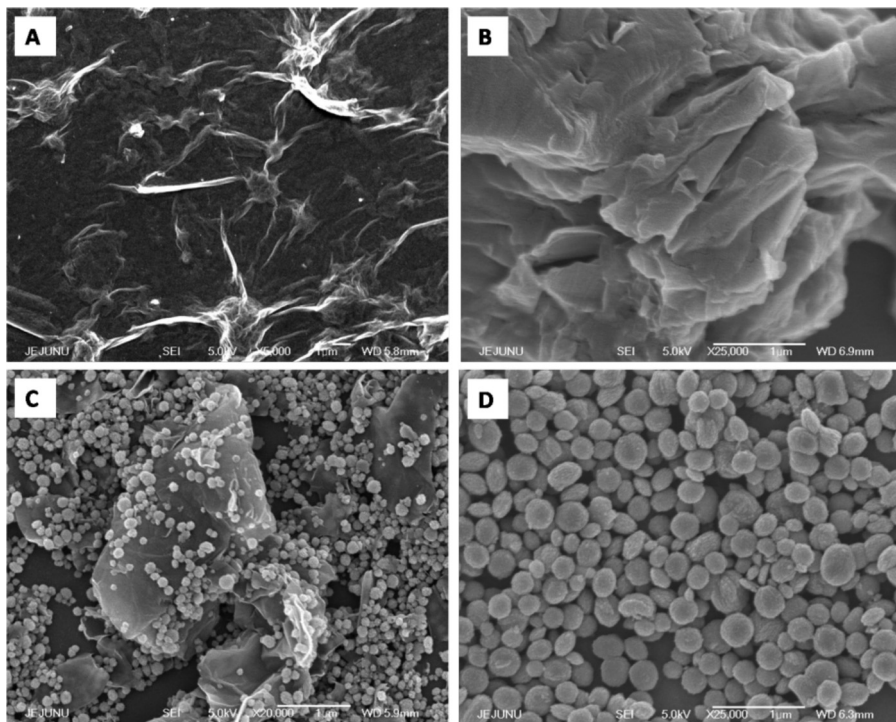
Fig. 1. FE-SEM micrographs of (A) GO, (B) rGO, (C) Fe_2O_3/rGO and (D) Fe_2O_3.

were well indexed to the rhombohedral crystal structure of Fe_2O_3 (JCPDS: 89-2810). All the peaks observed in the composites are related to the Fe_2O_3 (as shown in Fig. 2d) and the characteristic peaks of rGO nanosheets are not observed, this is due to the fact that the Fe_2O_3 nanoparticles are decorated on either side of the two dimensional thin rGO nanosheets.

Fig. S1 depict the FT-IR spectra of the GO (curve a), rGO (curve b), Fe_2O_3/rGO (curve c) and Fe_2O_3 (curve d). In the FT-IR spectrum of GO, the peak at 3440 and 1629 cm^{-1} are attributed to O—H stretching and bending vibrations, respectively. The other oxygen containing functional groups are revealed by the bands at 1728 (C=O stretching in COOH), 1060 (C—O stretching), 1241 (C—OH stretching) and 1382 cm^{-1} (C—O—C stretching in epoxy). In Fig. S1b and c the intensity of the oxygen-containing functional groups were greatly suppressed and some peaks were disappeared when compared to the GO peaks due to fact that the GO reduced to rGO. It is also noted that the new vibration bands appear at 474 and 574 cm^{-1} (Fe^{3+}—O^{2-} stretching vibration in the FeO_6 octahedron

and FeO_4 tetrahedron, respectively) for Fe_2O_3/rGO composite (curve c) [39], these two peaks were similar to Fe_2O_3 (curve d). These data indicate that the Fe_2O_3 nanoparticles were grafted onto the rGO sheets.

3.2. CV and EIS studies on Fe_2O_3/rGO modified GC electrode

The cyclic voltammogram (CV) curves of the bare GC (curve a), rGO (curve b), Fe_2O_3/rGO (curve c) and Fe_2O_3 (curve d) modified electrodes recorded in the presence of 1 mM $[Fe(CN)_6]^{3-/4-}$ in 0.1 M KCl at a scan rate 50 mV s^{-1} are shown in Fig. 3A. Modification of the rGO (curve b) onto the GC electrode surface increase the peak current of $[Fe(CN)_6]^{3-/4-}$ (i_{pa}: 21.1 μA) compared to the unmodified GC (curve a) electrode (i_{pa}: 19.2 μA). This could be attributed to the sheets like structure of rGO with high surface area and good electrical conductivity which facilitate the $[Fe(CN)_6]^{3-/4-}$ redox reaction. On the other hand, modification of the Fe_2O_3/rGO (curve c) onto the GC electrode significantly enhance the redox peak current of
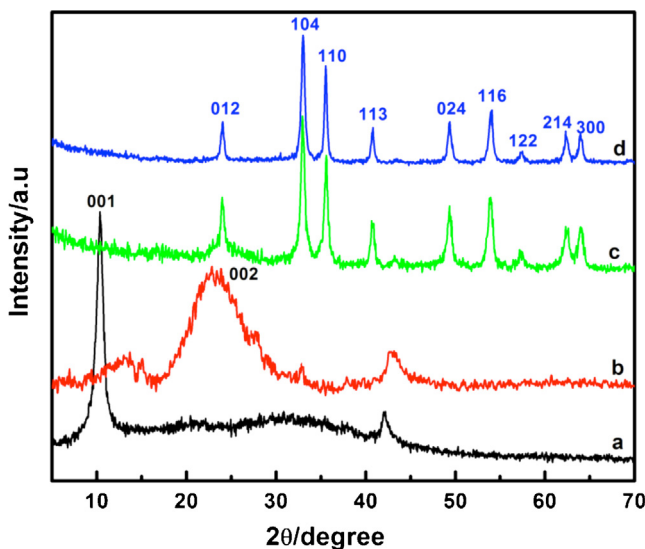
**Fig. 2.** X-ray diffraction patterns of (a) GO, (b) rGO, (c) Fe$_2$O$_3$/rGO and (d) Fe$_2$O$_3$.

rGO sheet and also restrict the formation of face-to-face stacking in rGO sheets. These results indicate that the newly formed Fe$_2$O$_3$/rGO composite have newer functionalities which are different from those of single component nano materials. The electrochemical behavior of bare GC and modified electrodes were further investigated in 0.1 M KCl solution containing 1 mM [Fe(CN)$_6$]$^{3-/4-}$ as a redox probe. Fig. S2 shows various cyclic voltammograms recorded at different scan rates (10–100 mV s^{-1}) for bare GC (A), rGO (B), Fe$_2$O$_3$/rGO (C) and Fe$_2$O$_3$ (D) modified electrodes. It can be seen that the anodic and cathodic peak current increases with increasing scan rates (10–100 mV s^{-1}). Further, a good linearity was obtained while plotting the current against square root of scan rate (inset of Fig. S2), indicating that the oxidation of [Fe(CN)$_6$]$^{3-/4-}$ was diffusion controlled process.

The charge transport process of the Fe$_2$O$_3$/rGO modified GC electrode was studied by monitoring charge transfer resistance (R_{ct}) at the electrode/electrolyte interface. The value of charge transfer resistance ($R_{ct}\Omega$) were obtained by Randels equivalent circuit, R_s ($Q_{CPE}(R_{ct}W)$), where R_s is the solution resistance, R_{ct} is the charge transfer resistance, W is the Warburg impedance and Q_{CPE} is the constant phase element (CPE) (Table S1). Fig. 3B shows the electrochemical impedance spectroscopy (EIS) responses of the bare and modified GC electrodes. The value of the charge transfer resistance (R_{ct}) for the bare GC (curve a), rGO (curve b), Fe$_2$O$_3$/rGO (curve c) and Fe$_2$O$_3$ (curve d) modified electrodes were estimated to be 161, 95, 58 and 2445 Ω (as given in (Table S1)), respectively. The

[Fe(CN)$_6$]$^{3-/4-}$ (i_{pa}: 24.5 µA) compared to bare GC, rGO and Fe$_2$O$_3$ (i_{pa}: 21.1 µA, curve d) modified GC electrodes due to the catalytic properties of Fe$_2$O$_3$ nanoparticles were uniformly grafted over the
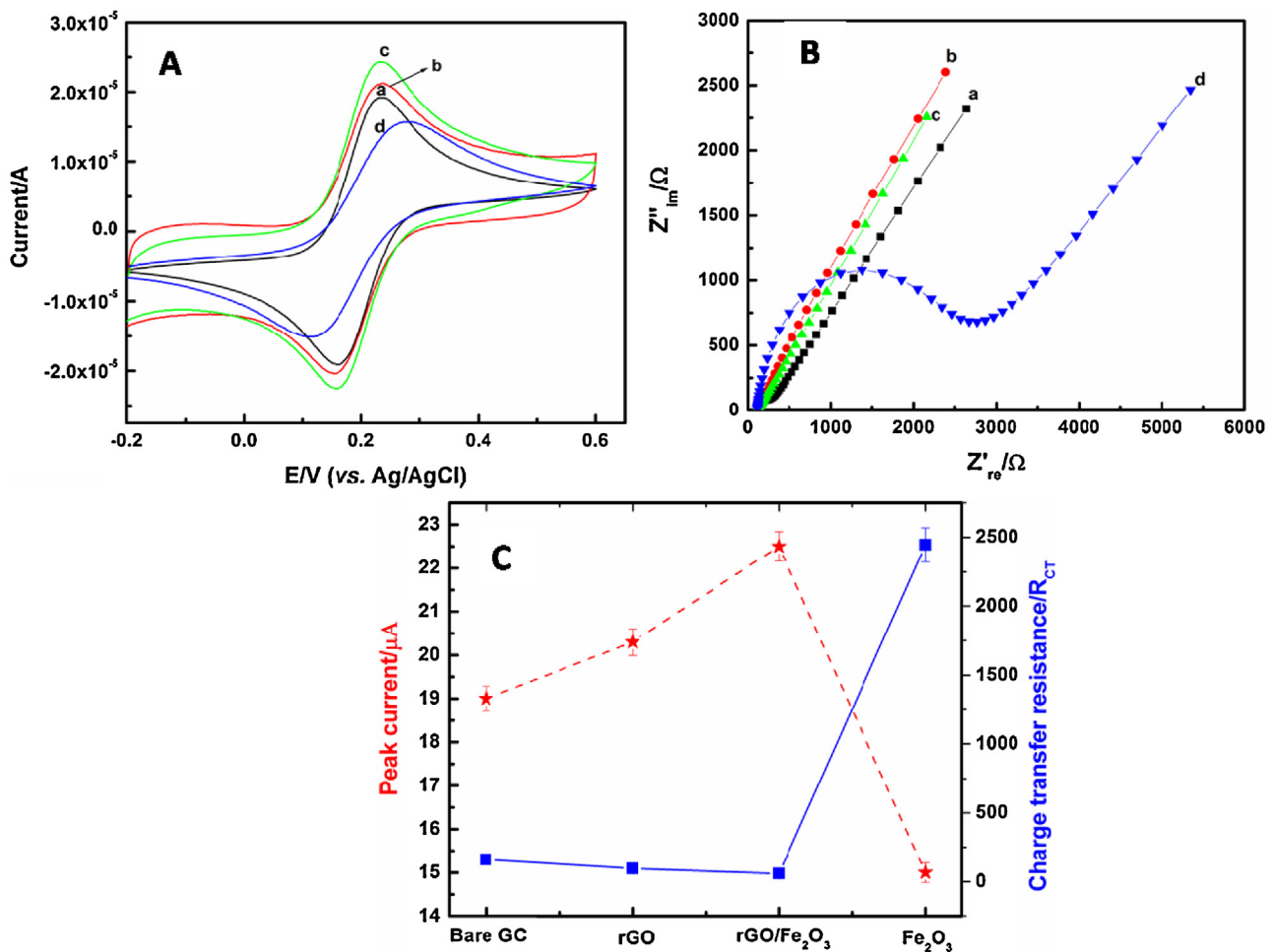
Fig. 3. A CV behavior of the modified GC electrodes in presence of 1 mM [Fe(CN)$_6$]$^{3-/4-}$ in 0.1 M KCl at a scan rate of 50 mV s^{-1}. (B) EIS behavior of the modified GC electrodes measured by impedance in the frequency region from 100 KHz to 0.1 Hz at a DC potential of 200 mV and AC potential of ±10 mV in presence of 1 mM [Fe(CN)$_6$]$^{3-/4-}$ in 0.1 M KCl. Curve a: bare GC, curve b: rGO, curve c: Fe$_2$O$_3$/rGO and curve d: Fe$_2$O$_3$ modified electrodes. (C) Plot of peak current and charge transfer resistance against different modified GC electrodes.
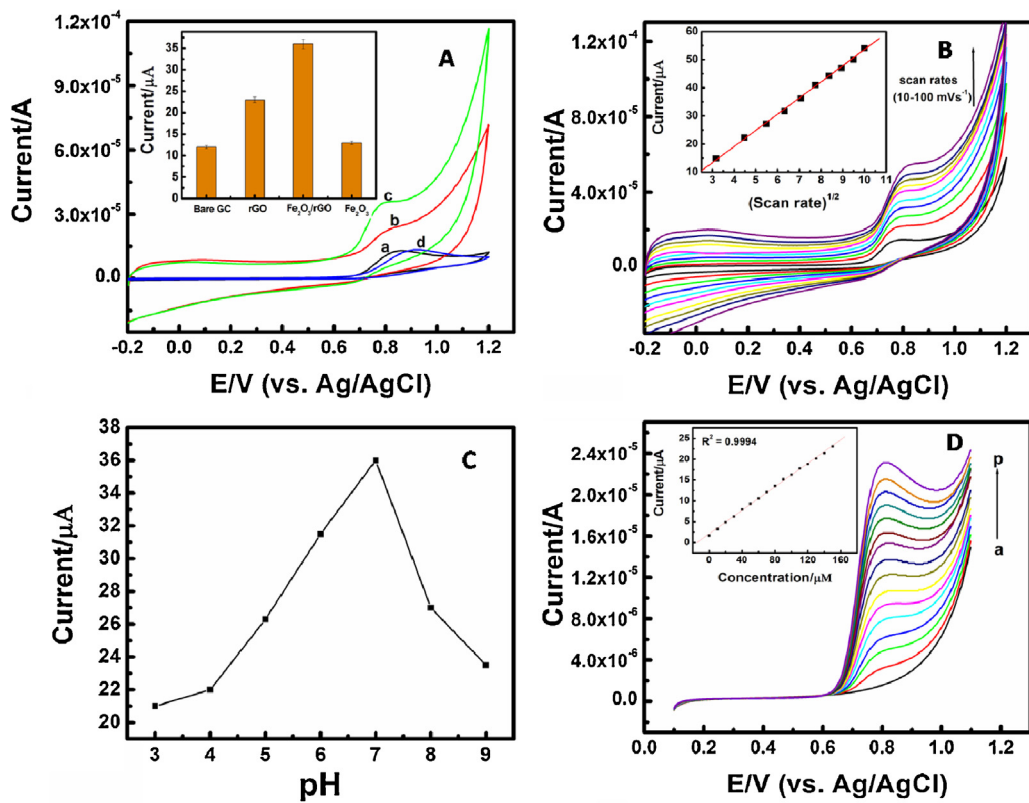
Fig. 4. A CVs obtained for nitrite (3.0×10^{-4} M) at the (a) bare GC, (b) rGO, (c) Fe_2O_3/rGO and (d) Fe_2O_3 modified electrode recorded in PB solution (pH 7.0) at a scan rate of 50 mV s^{-1} at a potential between −0.2 and 1.2 V, Inset: bar diagram of peak current against modified electrodes (B) CVs obtained for nitrite (3.0×10^{-4} M) at the Fe_2O_3/rGO modified electrode at different scan rates (10–100 mV s^{-1}) in PB solution (pH 7.0), Inset shows the resulting calibration plot. (C) Plot of oxidation peak current of nitrite *vs.* pH (D) LSVs obtained for nitrite in the concentrations ranging from 0 to 150 µM. Nitrite was added in steps of 10 µM each at the Fe_2O_3/rGO modified electrode in PB solution (pH 7.0).

R_{ct} value of Fe_2O_3/rGO modified GC electrode is lower than that of bare GC, rGO and Fe_2O_3 modified electrodes. These results were demonstrate that Fe_2O_3/rGO modified electrode can form good electron pathways between the electrode and electrolyte and can be required to be a good platform for sensing applications. These results are in good agreement with the peak current (i_{pa}) values obtained from CVs measurements (Fig. 3C). Hence we have used Fe_2O_3/rGO modified GC electrode for further investigation.

3.3. Electrochemical determination of nitrite

The main objective of the present work is to utilize the Fe_2O_3/rGO modified GC electrode for the electrochemical determination of nitrite. Fig. 4A shows the CVs obtained for 3.0×10^{-4} M nitrite in 0.1 M PB solution (pH 7.0) at bare GC (curve a), rGO (curve b), Fe_2O_3/rGO (curve c) and Fe_2O_3 (curve d) modified electrodes at a scan rate of 50 mV s^{-1}. Compared to those obtained at the bare GC (12 µA), rGO (23 µA) and Fe_2O_3 (13 µA) modified electrodes, a remarkably larger peak current was obtained at the Fe_2O_3/rGO modified electrode (36 µA). This anodic peak current obtained for the Fe_2O_3/rGO modified electrode is nearly 3.0, 1.5 and 2.8 fold higher when compared to the bare GC, rGO and Fe_2O_3 modified GC electrodes, respectively (inset of Fig. 4A). It is also noted that the oxidation peak potential for Fe_2O_3/rGO modified electrode was 80 mV less positive potential than the bare GC electrode. Two factors contributing to the increased peak current and decreased oxidation potential of nitrite for the Fe_2O_3/rGO modified electrode surface are: (i) the Fe_2O_3/rGO composite restrict the rGO sheets aggregation by the introduction of Fe_2O_3 nanoparticles on both sides of the rGO sheets and hence, increase the surface area of Fe_2O_3/rGO composite than that of rGO sheet alone. (ii) The Fe_2O_3

nanoparticles in the Fe_2O_3/rGO composite are well dispersed, electrochemically accessible and highly active. These data indicate that the Fe_2O_3/rGO modified GC electrode has a good catalytic activity toward nitrite sensing compared to that of the bare GC, rGO and Fe_2O_3.

The Fe_2O_3/rGO modified GC electrode did not show any oxidation response in the absence of nitrite (Fig. S3). The observed oxidation peak for nitrite in Fig. 4A is due to the two-electron oxidation of NO_2^- to NO_3^- [40]. The oxidation reaction process can be derived through an electrocatalytic mechanism involving the Fe(III)/Fe(II) ion centers, and the catalytic mechanism of the Fe_2O_3/rGO to nitrite oxidation can be explained by the following scheme; the voltammetric response of nitrite at the Fe_2O_3/rGO modified electrode is due to two steps, *viz.*, an electrochemical process followed by a chemical reaction. In the first step, Fe(II) was electrochemically oxidized to Fe(III) (Eq. (1)) and in the second step NO_2^- was chemically oxidized to NO_3^- by Fe(III) (Eq. (2))

$$2Fe(II) \rightarrow 2Fe(III) + 2e^- \qquad (1)$$

$$2Fe(III) + NO_2^- \rightarrow 2Fe(II) + NO_3^- \qquad (2)$$
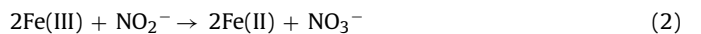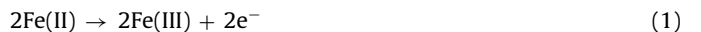
Further, the effect of scan rate on the electrocatalytic oxidation of 3.0×10^{-4} M nitrite at the Fe_2O_3/rGO modified GC electrode was investigated by CV. The oxidation peak currents (i_{pa}) increased gradually with the increase of scan rates (ν) (10–100 mV s^{-1}) in 0.1 M PB (pH 7.0) solution are shown in Fig. 4B. A good linearity was obtained while plotting the current against square root of scan rate with a correlation coefficient of 0.9991 (inset of Fig. 4B), indicating that the oxidation of nitrite was diffusion controlled process.

The influence of solution pH on the electrochemical response of nitrite (3.0×10^{-4} M) at the Fe_2O_3/rGO modified electrode was

Table 1
Comparison of different chemically modified electrodes for the determination of nitrite with Fe_2O_3/rGO modified electrode.

Electrode material	Linear range (μM)	Detection limit (μM)	Sensitivity (μA/μM)	Ref.
[a]IL-SWCNT	1.0–12,000	0.1	0.07985	[15]
[b]PEDOT/AuNP	3.0–300	0.1	–	[16]
[c]POA	2.0–50	1.05	–	[17]
β-MnO$_2$	0.29–26090	0.29	0.00121	[18]
Au/ZnO/MWCNTs	0.78–400	0.4	–	[19]
[d]Cu-NDs/rGO	1.25–13000	0.4	0.214	[23]
Pd/rGO	0.04–108	0.01564	7.62	[24]
[e]PDDA/P$_2$W$_{17}$V-CNTs	0.05–2130	0.0367	0.350	[44]
Fe-HNPs[f]	9.0–3000	2.6	0.01983	[45]
Cu$_{nano}$/CNTs/CS[g]	0.1–2500	0.024	0.04892	[46]
nanoAu/Ch[h]	0.4–750	0.1	0.354	[40]
Fe$_2$O$_3$/rGO	0.05–780	0.015	0.204	This work

[a] Ionic liquid.
[b] Poly(3,4-ethylenedioxythiophene).
[c] Poly(o-anisidine).
[d] Copper nanodendrites.
[e] Poly(diallyldimethylammonium chloride).
[f] Hematite nano-polyhedrons.
[g] Chitosan.
[h] Choline chloride.
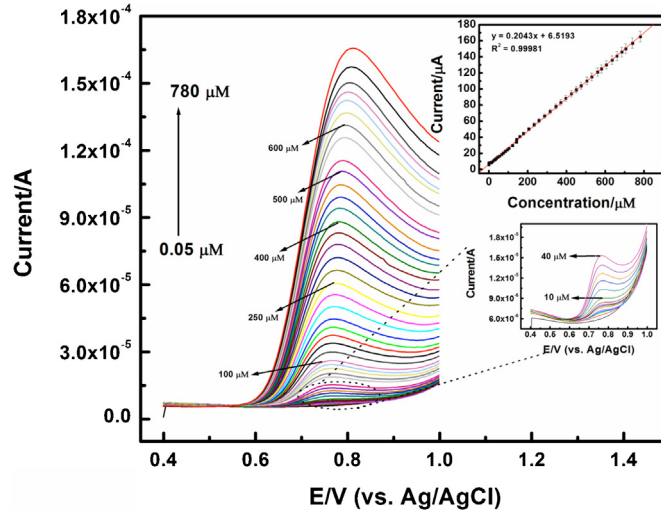
Fig. 5. DPVs of the Fe_2O_3/rGO modified GC electrode in PB solution (pH 7.0) with various concentrations of nitrite (0.05–780 μM), scan rate 10 mV s^{-1}; amplitude 0.025 V and step potential 0.05 V. Inset shows the resulting calibration plot.

examined by recording CVs in PBS (pH 3.0–9.0) at a scan rate of 50 mV s^{-1}. As shown in Fig. 4C, the oxidation peak current of nitrite was greatly influenced by solution pH and the peak currents gradually increased with pH in the range of 3.0–7.0. The maximum peak currents were obtained at the pH of 7.0 due to the fact that the instability of nitrite anions in acidic medium (<6.0) (decomposition of NO_2^- into NO_3^-) [41]. Further, the oxidation of nitrite became more difficult at high pH (>7.0) due to the lack of protons [42]. Therefore, a PB solution with pH 7.0 was chosen for the rest of the electrochemical sensing of nitrite in this work.

Fig. 4D shows the linear sweep voltammograms (LSVs) obtained for nitrite in the concentration range of 0–150 μM at the Fe_2O_3/rGO modified GC electrode. The oxidation current of nitrite increased with a slight negative potential shift in the oxidation peak potential upon each increment of 10 μM. The oxidation currents had a linear relationship with the concentration of nitrite with a correlation coefficient of 0.9994 (inset of Fig. 4D).

Furthermore, DPV was performed under the optimum conditions to examine the sensitivity of the Fe_2O_3/rGO modified GC electrode toward the detection of nitrite in static solutions. The DPV is a pulse technique which allows much higher sensitivity

than conventional sweep techniques when detecting very low concentrations of an analyte. Fig. 5 depicts the DPV curves of the Fe_2O_3/rGO modified electrode in PB solution (pH 7.0) for different concentrations of nitrite. Here the DPVs were recorded by sweeping the potential between 0.4 and 1.0 V at amplitude of 0.025 V, a step potential of 0.05 V and a scan rate of 10 mV s^{-1}. In Fig. 5, DPV curves shows the well-defined and stable anodic oxidation peak current curves for nitrite. These results demonstrated that the Fe_2O_3/rGO modified electrode might provide a good electrocatalytic activity toward nitrite sensing. Further, the DPV current response was increased linearly with increasing nitrite concentration in the range of 0.05–780 μM (Fig. 5) with a correlation coefficient of 0.9998, and the Fe_2O_3/rGO modified electrode displayed an excellent sensitivity for nitrite detection with detection limit of 0.015 μM. The linear range, detection limit and sensitivity for nitrite at Fe_2O_3/rGO modified electrode compared with the recently reported chemically modified electrodes (Table 1). As, mentioned above, the maximum limit of nitrite in drinking water is 3 mg L^{-1}. Therefore, the Fe_2O_3/rGO modified electrode is more suitable for the determination of nitrite in real water samples.

3.4. Selective determination of nitrite in the presence of interfering compounds using the Fe_2O_3/rGO composite modified electrode

The anti-interference ability of the Fe_2O_3/rGO composite was tested toward the detection of nitrite from various common ions such as Mg^{2+}, Ca^{2+} Na^+ and Cu^{2+} and some physiological interferents such as glucose, hydrogen peroxide and urea. No change in the DPV current response was observed for 0.03 mM nitrite in the presence of 0.3 mM of glucose, hydrogen peroxide and urea; and 3 mM of $MgCl_2$, $CaCl_2$, NaCl and $CuCl_2$. Results summarized in supplementary Table S2, shows that the present modified electrode is highly selective toward the determination of nitrite even in the presence of 100-fold excess of these interferents.

3.5. Reproducibility and stability measurements

In order to investigate the stability of the Fe_2O_3/rGO composite modified electrode, the DPVs for 1.25×10^{-4} M nitrite in a 0.1 M PB solution were recorded for every 10 min interval. It was found that the oxidation peak current remained the same with a relative standard deviation of 2.20% for 15 repetitive measurements. After DPV measurements, the electrode was kept in a PB solution

Table 2
Determination of nitrite at various concentrations in tap water.

Sample	Added (μM)	Found (μM)	Recovery (%)	R.S.D. ($n = 3$) (%)
1	40	40.03	101	2.79
2	80	82.00	102.50	1.14
3	120	118.84	99.03	0.96

at room temperature. The current response decreased about 0.97% in 5 days and 1.94% in about 10 days. These results indicate that the Fe_2O_3/rGO modified electrode has a good stability, reproducibility and does not undergo surface fouling. To ascertain the reproducibility of the results, five different GC electrodes were modified with the Fe_2O_3/rGO and their response toward the oxidation of 2.25×10^{-4} M nitrite was tested. The peak current obtained in the measurements of four independent electrodes showed a relative standard deviation of 1.23%, confirming that the results are reproducible. The above results show that the fabricated nitrite sensor is very stable and reproducible.

The practical application of the Fe_2O_3/rGO composite modified GC electrode was tested to determine the concentrations of nitrite in tap water sample. The tap water sample was prepared following the report by Qin et al. [43] and the results are summarized in Table 2. It can be clearly observed that a good recovery was obtained suggesting the practical applicability of the proposed method. The main advantages of the newly fabricated nitrite sensor is that the Fe_2O_3/rGO composite preparation (eco-friendly hydrothermal approach) and electrode modification procedure adopted in the present study is very simple when compared to the literature reports. The performance of the fabricated nitrite sensor is very much comparable to the literature values (Table 1). It is evident from Table 1, the designed Fe_2O_3/rGO modified electrode exhibited relatively low detection limit, high sensitivity and wide linear range. The superiority of the present sensor can be attributed to the fact that the high electrical conductivity and large surface area.

4. Conclusion

We have demonstrated the synthesis of Fe_2O_3/rGO composite by an environment-friendly approach and their application in voltammetric determination of nitrite in neutral medium. The Fe_2O_3/rGO modified electrode provided a sheet like structure with large effective surface area, which could act as electron transfer medium and promote the charge transfer between electrode surface and nitrite. The sensitivity and detection limit for the fabricated nitrite electrochemical sensor have been found to be 0.204 μA μM^{-1} and 0.015 μM, respectively. Excellent performance in sensitivity, stability, reproducibility and selectivity was achieved when the sensor was exposed to nitrite solution. All these advantageous features can make the proposed sensor applicable in environmental, food or other areas.

Acknowledgement

Appendix A. Supplementary data

Supplementary data associated with this article can be found, in the online version, at http://dx.doi.org/10.1016/j.apcatb.2013.10.044.

References

[1] M.J. Moorcroft, J. Davis, R.G. Compton, Talanta 54 (2001) 785–803.
[2] I. Mikami, Y. Sakamoto, Y. Yoshinaga, T. Okuhara, Appl. Catal. B: Environ. 44 (2003) 79–86.
[3] B. Bems, F.C. Jentoft, R. Schlogl, Appl. Catal. B: Environ. 20 (1999) 155–163.
[4] S. Jacinto, J.A. Anderson, Appl. Catal. B: Environ. 77 (2008) 409–417.
[5] WHO (World Health Organization), Guide Lines for Drinking-Water Quality, vol. 1, 3rd ed., World Health Organization, Geneva, 2004.
[6] K. Nakamura, Y. Yoshida, I. Mikami, T. Okuhara, Appl. Catal. B: Environ. 65 (2006) 31–36.
[7] W. Lijinsky, S.S. Epstein, Nature 225 (1970) 21–23.
[8] S.S. Mirvish, Cancer Lett. 93 (1995) 17–48.
[9] M. Bru, M.I. Burguete, F. Galindo, S.V. Luis, M.J. Marin, L. Vigara, Tetrahedron Lett. 47 (2006) 1787–1791.
[10] P. Mikuska, Z. Vecera, Anal. Chem. Acta 495 (2003) 225–232.
[11] X. Wang, E. Adams, A. Van Schepdael, Talanta 97 (2012) 142–144.
[12] H. Kodamatani, S. Yamazaki, K. Saito, T. Tomiyasu, Y. Komatsu, J. Chromatogr. A 1216 (2009) 3163–3167.
[13] S. Radhakrishnan, C. Sumathi, A. Umar, S.J. Kim, J. Wilson, V. Dharuman, Biosens. Bioelectron. 47 (2013) 133–140.
[14] M. Veerapandian, Y.-T. Seo, H. Shin, K. Yun, M.-H. Lee, Int. J. Nanomed. 7 (2012) 6123–6136.
[15] L. Zhou, J.-P. Wang, L. Gai, D.-J. Li, Y.-B. Li, Sens. Actuators B 181 (2013) 65–70.
[16] O. Zhang, Y. Wen, J. Xu, L. Lu, X. Duan, H. Yu, Synth. Met. 164 (2013) 47–51.
[17] R. Ojani, J.-B. Raoof, S. Zamani, Appl. Surf. Sci. 271 (2013) 98–104.
[18] J.J. Feng, P.P. Zhang, A.J. Wang, Y. Zhang, W.J. Dong, J.R. Chen, J. Colloid Interface Sci. 359 (2011) 1–8.
[19] A.J. Lin, Y. Wen, LJ. Zhang, B. Lu, Y. Li, Y.Z. Jiao, H.F. Yang, Electrochim. Acta 56 (2011) 1030–1036.
[20] Y. Qian, F. Ye, J. Xu, Z.G. Le, Int. J. Electrochem. Sci. 7 (2012) 10063–10073.
[21] S.J.R. Prabakar, Y.H. Hwang, E.G. Bae, S. Shim, D. Kim, M.S. Lah, K.S. Sohn, M. Pyo, Adv. Mater. 25 (2013) 3307–3312.
[22] Z.S. Wu, W.C. Ren, L. Wen, L.B. Gao, J.P. Zhao, Z.P. Chen, G.M. Zhou, F. Li, H.M. Cheng, ACS Nano 4 (2010) 3187–3194.
[23] D. Zhang, Y. Fang, Z. Miao, M. Ma, X. Du, S. Takahashi, J. Anzai, Q. Chen, Electrochim. Acta 107 (2013) 656–663.
[24] Y. Zhang, Y. Zhao, S. Yuan, H. Wang, C. He, Sens. Actuators B 185 (2013) 602–607.
[25] L. Cui, J. Zhu, X. Meng, H. Yin, X. Pan, S. Ai, Sens. Actuators B 161 (2012) 641–647.
[26] G. Neri, A. Bonavita, S. Galvagno, P. Siciliano, S. Capone, Sens. Actuators B 82 (2002) 40–47.
[27] C. Feldmann, Adv. Mater. 13 (2001) 1301–1303.
[28] W. Weiss, D. Zscherpel, R. Schlogl, Catal. Lett. 52 (1998) 215–220.
[29] F. Bondioli, A.M. Ferrari, C. Leonelli, T. Manfredini, Mater. Res. Bull. 33 (1998) 723–729.
[30] M. Fukazawa, H. Matuzaki, K. Hara, Sens. Actuators B 14 (1993) 521–522.
[31] Y. Zhou, Q. Bao, L.A.L. Tang, Y. Zhong, K.P. Loh, Chem. Mater. 21 (2009) 2950–2956.
[32] Y. Zhu, S. Murali, M.D. Stoller, A. Velamakanni, R.D. Piner, R.S. Ruoff, Carbon 48 (2010) 2118–2122.
[33] Z. Lei, L. Lu, X.S. Zhao, Energy Environ. Sci. 5 (2012) 6391–6399.
[34] A.V. Murugan, T. Muraliganth, A. Manthiram, Chem. Mater. 21 (2009) 5004–5006.
[35] K. Krishnamoorthy, G.S. Kim, S.-J. Kim, Ultrason. Sonochem. 20 (2013) 644–649.
[36] K. Krishnamoorthy, M. Veerapandian, K. Yun, S.-J. Kim, Carbon 53 (2013) 38–49.
[37] J. Zhu, T. Zhu, X. Zhou, Y. Zhang, X.W. Lou, X. Chen, H. Zhang, H.H. Hng, Q. Yan, Nanoscale 3 (2011) 1084–1089.
[38] D.Y. Pan, S. Wang, B. Zhao, M.H. Wu, H.J. Zhang, Y. Wang, Z. Jiao, Chem. Mater. 21 (2009) 3136–3142.
[39] H.D. Ruan, R.L. Frost, J.T. Kloprogge, L. Duong, Spectrochim. Acta A 58 (2002) 967–981.
[40] P. Wang, Z. Mai, Z. Dai, Y. Li, X. Zou, Biosens. Bioelectron. 24 (2009) 3242–3247.
[41] O. Brylev, M. Sarrazin, L. Roue, D. Belanger, Electrochim. Acta 52 (2007) 6237–6247.
[42] W.L. Sun, S. Zhang, H.Z. Liu, L.T. Jin, J.L. Kong, Anal. Chim. Acta 388 (1999) 103–110.
[43] C. Qin, W. Wang, C. Chen, L. Bu, T. Wang, X. Su, Q. Xie, Z. Yao, Sens. Actuators B 181 (2013) 375–381.
[44] D. Zhang, H. Ma, Y. Chen, H. Pang, Y. Yu, Anal. Chim. Acta 792 (2013) 35–44.
[45] C. Xia, X. Yanjun, W. Ning, Electrochim. Acta 59 (2012) 81–85.
[46] S. Yang, X. Liu, X. Zeng, B. Xia, J. Gu, S. Luo, N. Mai, W. Wei, Sens. Actuators B 145 (2010) 762–768.